Direct Simulation of Thermal Conductivity by Molecular Dynamics

Philip B. Allen[1,*] and Yerong Li[2,†]

[1] *Physics and Astronomy Department, Stony Brook University, Stony Brook, NY 11794-3800, USA*
[2] *Department of Intensive Instruction, Nanjing University, Nanjing 210093, China*

(Dated: October 26, 2014)

Classical molecular dynamics (MD) is often used to simulate thermal conductivity (κ) by a "direct method" where a steady state heat current and corresponding temperature gradient are created computationally over a simulation cell of thousands of atoms. This paper presents a variation of such algorithms, that gives directly $\kappa(q)$, the Fourier transform of the non-local $\kappa(x-x')$ that relates $J(x)$ to $\nabla T(x')$. The algorithm is tested on the Lennard-Jones liquid and crystal, and shown to be quite efficient. Knowledge of $\kappa(q)$ permits a controlled extrapolation to the macroscopic κ, the $q \to 0$ limit of $\kappa(q)$. The nature of this extrapolation is studied using a Debye spectrum and frequency-dependent relaxation rate $1/\tau_Q \propto \omega_Q^2$. The aim of extrapolation is to reduce the error from the finite length of the simulation cell. Errors associated with the finite width of the simulation cell are also analyzed using the same Debye spectrum.

I. INTRODUCTION

Molecular dynamics (MD) simulation works for insulators at temperature T high enough that quantum lattice dynamics is well approximated by classical Newtonian trajectories. It has the advantage of treating interatomic forces beyond harmonic theory without requiring perturbation theory. For thermal conductivity[1,2] $\kappa = \mathrm{Lim}_{q\to 0}\kappa(q)$ of a crystal[3], the biggest difficulty is that small ω_Q modes have long mean free paths Λ_Q. This means that the current J at one location x depends on temperature T and temperature gradient $-\nabla T$ at distant locations x'. The relation between $J(x)$ and $-\nabla T(x')$ is the non-local conductivity $\kappa(x-x')$. The long range of $|x-x'|$ means rapid variation of $\kappa(q)$ with q and difficulty taking the $q \to 0$ limit.

Although non-locality of κ is certainly implicitly acknowledged, it is rarely[4] regarded as a direct topic of study. The main methods of MD used for κ are the Green-Kubo (GK) and the "direct method" (DM), also known as "non-equilibrium molecular dynamics" (NEMD). These are compared, for example, in Ref.2. The former computes κ *via* equilibrium fluctuations averaged over a large supercell with periodic boundaries. The latter involves external heat which drives the system from equilibrium. The unit cell is elongated in the direction of heat flow, and periodic in the perpendicular directions. Equal heat input and output allows a steady state. Heating and cooling are isolated in separate regions, and "bulk" conduction occurs in between, if the separation is large enough.

Here we argue that a direct study of $\kappa(q)$ is both warranted and useful for finding the bulk $\kappa = \mathrm{Lim}_{q\to 0}\kappa(q)$ by NEMD. The Peierls-Boltzmann equation (PBE) is well adapted[3] for study of $\kappa(q)$. This paper does four things. First, a particular version of the standard DM is analyzed, where the long direction of heat flow is also treated with periodic boundaries (with length L, and discrete slabs perpendicular.) Heat is added in one slab, and removed at an equal rate from another slab a distance $L/2$ away, fixing the steady state heat current J. The thermal conductivity $\kappa_{\mathrm{eff}}(L)$ is the of ratio of J to the temperature gradient $-\nabla T(\mathrm{mid})$ at the mid-point. A rigorous, but complicated, relation between $\kappa_{\mathrm{eff}}(L)$ and $\kappa(q)$ is worked out. Second, a method is developed for direct MD simulation of $\kappa(q)$, by applying and extracting heat in a sinusoidal pattern. This allows a better-controlled approach to the bulk limit. The present method, proposed previously in Ref.3, uses continuous heating in a sinusoidal pattern. We argue that this method also has numerical advantages over more traditional simulation protocols. Third, convergence of $\kappa(q)$ towards κ is studied by "direct method" simulation for the Lennard-Jones (LJ) liquid and crystal. Fourth, $\kappa(q)$ is studied by the PBE, using a Debye approximation ($\omega_Q = v|\vec{Q}|$ and $1/\tau_Q = (1/\tau_D)(\omega_Q/\omega_D)^2$). This is used to analyze convergence as a function of MD simulation-cell size.

II. PRELIMINARIES

This paper assumes a simulation cell with periodic boundary conditions. The atom at $\vec{r}$ and the atom at $\vec{r}+\vec{R}$ are equivalent, and have the same dynamics. For simplicity, the primitive translation vectors $\vec{R}$ of the simulation cell ($\vec{A}_1,\ \vec{A}_2,\ \vec{A}_3$), are assumed orthogonal. For example, in the sample calculations presented later, they are taken to be $N_1 a\hat{x},\ N_2 a\hat{y},\ N_3 a\hat{z}$, where a is the lattice constant, the edge-length of the *fcc* conventional cube. A typical cell has size ($N_1,\ N_2,\ N_3$) = (6, 6, 80); with 4 atoms in the conventional cube, this means 11,520 atoms. Heating is done in slabs perpendicular to the long vector $\vec{A}_3$. Therefore, current flows parallel to $\vec{A}_3$, and $L = |\vec{A}_3| = N_3 a$ is chosen as large as computation permits, trying to surpass the distance Λ of non-local thermal memory.

Boundaries create challenging problems. Nanoscale heat transfer is typically dominated by thermal boundary (or Kapitza) resistance[6]. For study of bulk conductivity, the aim is to reduce the influence of boundaries. One

can argue[5] that periodic boundary conditions are not the most favorable way to do this. However, in this paper, the simplicity for analysis of periodicity overrules other considerations.

A further simplification follows computational necessity, and discretizes the temperature $T(\vec{r})$ into slab values $T(\ell)$. The slabs are layered in the $\vec{A}_3$-direction, and have width $d = n_S a$ where n_S is a small integer and a factor of N_3. The number of slabs is $N_S = N_3/n_S$. Let the variable x denote distance along the $\vec{A}_3$-axis, perpendicular to slabs. The slab indexed by the integer ℓ is located in the interval $x = \ell d \pm d/2$. The temperature $T(\ell)$ is found from the average kinetic energy of the atoms in the ℓ'th slab. Heat is transferred externally into the ℓ'th cell at a volume-average rate $\dot{e}(\ell)$. In steady state, this is balanced by an outward flux $[J(\ell+1/2) - J(\ell-1/2)]/d$. Both current and temperature gradient are properties of the junction of two adjacent slabs. Their steady-state linear relation is $J(\ell+1/2) = -\sum_{\ell'} \kappa(\ell,\ell')\nabla T(\ell'+1/2)$, where the sum runs over the N_S slabs. This definition is required by linear math. Periodicity requires $\kappa(\ell,\ell') = \kappa(\ell + mN_S, \ell' + nN_S)$ and homogeneity (if the medium is in fact homogeneous) requires that $\kappa(\ell,\ell') = \kappa(\ell - \ell')$. Corresponding (*via* a unitary Fourier transformation) to the N_S distinct slabs, there are N_S distinct wave-vectors $q = 2\pi n_q/N_S d$, indexed by integers n_q and distributed in a one-dimensional Brillouin zone. In the homogeneous case, the relation is $J(q) = -\kappa(q)\nabla T(q)$. We will use the same symbols ($\nabla T(\ell)$ and $\nabla T(q)$, for example) for both coordinate space and reciprocal space representations of the functions, needing the coordinate ℓ or q to clarify which representation. These ideas were introduced in Ref. 3, where further properties are explained.

It is not hard to extend the usual derivation of the Kubo formula (ref. 7, for example) to derive a Kubo formula for $\kappa(x,x')$ or $\kappa(\ell,\ell')$. The classical limit is

$$\kappa(\ell,\ell') = -\frac{1}{k_B T^2}\int_0^\infty dt < J(\ell+1/2,t)J(\ell'+1/2,0) > \tag{1}$$

III. DISCRETE PAIR HEATING

Here is a simple version of NEMD simulation. Energy is added only to slab $\ell = 0$ at a volume-average rate $\dot{e}$, and extracted only from slab $N_S/2$ at the same rate. Zhou *et al.*[10] did a careful study of κ for GaN by this method. They discuss, but do not completely resolve, the issue of how the answer scales with system size. Here we analyze this version with the use of periodic boundaries ($\ell = \ell + N_S$). Zhou *et al.* used rigid boundaries. Heat current $J_x(\ell+1/2) = \pm(d/2)\dot{e} \equiv \pm J$ flows across slab boundaries, the plus sign for ℓ to the right of an input and left of an output slab, and the minus sign for opposite cases. Adding periodic boundary conditions permits a simple Fourier representation of J_x,

$$\begin{aligned} J_x(q) &= \frac{1}{N_S}\sum_{\ell=0}^{N_S-1} e^{-iqx(\ell+1/2)} J_x(\ell+1/2) \\ &= \frac{J}{N_S}\sum_{\ell=0}^{N_S/2-1}\left[e^{-iqx(\ell+1/2)} - \text{c.c.}\right] \\ &= \frac{J}{N_S}\left(\frac{1-e^{-iqL/2}}{1-e^{iqd}}\right)e^{-iqd/2} - \text{c.c.} \\ &= \frac{J}{iN_S}\left[\frac{1-(-1)^{n_q}}{\sin(qd/2)}\right] \end{aligned} \tag{2}$$

At $q = 0$, the expression [ ] in the last line of Eq.(2) is ill-defined; the correct value is 0, as is also true for all q's with even n_q. Now let us analyze the approximate thermal conductivity,

$$\kappa_{\text{eff}}(L) \equiv -J/\nabla_x T(\text{mid}). \tag{3}$$

That is, the thermal conductivity is taken as the ratio of the actual current J, controlled by the heating rate $\dot{e}$, to the temperature gradient $-\nabla_x T(\text{mid})$ found midway between the heat input slab ($\ell = 0$) and output slab ($\ell = N_S/2$). This temperature gradient has the Fourier representation

$$\begin{aligned} \nabla_x\, T\ (\text{mid}) &= \sum_q e^{iqN_S d/4}\nabla_x T(q) \quad [N_S/4 = \text{half integer}] \\ &= \sum_q e^{iqN_S d/4}\cos(qd/2)\nabla_x T(q) \quad [N_S/4 = \text{integer}]. \end{aligned} \tag{4}$$

In the case $N_S/4 =$ integer, the slab $\ell = N_S/4$ lies midway between heat input and output, so the temperature gradient (needed at the slab mid-point) is taken as the average of the left and right slab boundaries. This introduces the factor $\cos(qd/2)$ in the second version of Eq.(4). Finally, we substitute $\nabla_x T(q) = -J_x(q)/\kappa(q)$ in Eq.(4), and use Eq.(2) for $J_x(q)$. Then Eq.(3) becomes

$$\begin{aligned} \frac{1}{\kappa_{\text{eff}}} &= \frac{2}{N_S}\sum_q^{n_q=\text{odd}} \frac{\sin(qL/4)}{\sin(qd/2)}\left[\frac{1 \text{ or } \cos(qd/2)}{\kappa(q)}\right] \\ &= \left[\frac{4 \text{ or } 4\cos(\pi/N_S)}{N_S\sin(\pi/N_S)}\right]\frac{1}{\kappa(q_{\min})} + \{|n_q| \geq 3 \text{ terms}\}. \end{aligned} \tag{5}$$

This is a surprisingly complicated relation between the size-dependent value of κ_{eff} and the Fourier representation $\kappa(q)$. From Eq.(5), the leading term (at small $q_{\min}d/2 = \pi d/L$) is $1/\kappa_{\text{eff}} = 4/\pi\kappa(q_{\min})$, with oscillatory corrections $\sum_{n=1}(4/\pi)(-1)^n/[(2n+1)\kappa((2n+1)q_{\min})]$. In the local limit, $\kappa(q) = \kappa$, Eq.(5) converges exactly to $\kappa_{\text{eff}} = \kappa$. For crystals, where long-range non-local behavior is caused by long-wavelength phonons, the answer (for finite N_S) is a less accurate approximation to κ than $\kappa(q_{\min})$. This motivates developing an algorithm for the direct study of $\kappa(q)$.

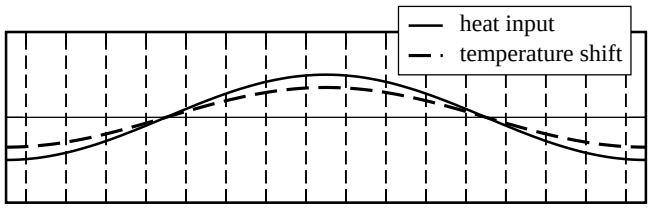

FIG. 1. Schematic picture of an $N_S = 16$ slab simulation cell with periodic boundary conditions. Heat is added or subtracted according to position, in the ℓ^{th} slab, as $\cos(2\pi\ell/N_S)$. The central cell is numbered $\ell = 0$. Temperature $T(\ell)$ is determined by averaging kinetic energy of atoms in each slab. In linear approximation, temperature must also vary as $\cos(2\pi\ell/N_S)$.

IV. SINUSOIDAL HEATING ALGORITHM

The simulation cell, divided into slabs, is shown schematically in Fig. 1. We want to modify the heat input profile. Instead of the two slab version, let the heat input be of the form $\dot{e}(\ell) = \dot{e}(q_{\min})\cos(q_{\min}x(\ell))$. The temperature variation then has the form $T(\ell) = T_0 + \Delta T\cos(q_{\min}x(\ell))$. Since slab temperatures $T(\ell)$ at all N_S values of ℓ are used to compute the Fourier amplitude ΔT, numerical noise averages out faster.

Equation 26 of the previous paper[3] says, for arbitrary heating $\dot{e}(\ell)$, heating rate, temperature, and conductivity in Fourier space are related by (for $q \neq 0$),

$$\Delta T(q) = \frac{\dot{e}(q)d^2}{4\sin^2(qd/2)\kappa(q)} \tag{6}$$

For simple sinusoidal heating, $\dot{e}(q)$ and $\Delta T(q)$ are zero except at $q = q_{\min}$. Then the conductivity is

$$\kappa(q_{\min}) = \frac{\dot{e}d^2/\Delta T}{4\sin^2(q_{\min}d/2)} \to \frac{N_S^2\dot{e}d^2}{4\pi^2\Delta T} \tag{7}$$

This makes sense: $\Delta T/N_S d$ measures the size of the temperature gradient, and $\dot{e}N_S d$, the heat input per unit area, measures the size of the heat current.

The question not yet addressed is, what is a good numerical algorithm to drive the oscillatory heat input? Our method for multi-slab sinusoidal heat input is related to the Müller-Plathe[8] algorithm for discrete slab heat input. The Müller-Plathe recipe is: find the hottest atom in the cold ($\ell = N_S/2$) slab, and the coldest atom in the hot ($\ell = 0$) slab. Interchange their velocities. Energy and momentum are both conserved, and the system is driven from equilibrium in a way that must be monitored. Cao and Li[9] among others, have suggested modified algorithms of this type.

In our method, driving is done by spatially periodic injection and simultaneous removal of heat. Examine a slab ℓ (with $0 \leq \ell < N_S/4$), and its conjugate slab $N_S/2-\ell$. The former is "hotter" than the latter because

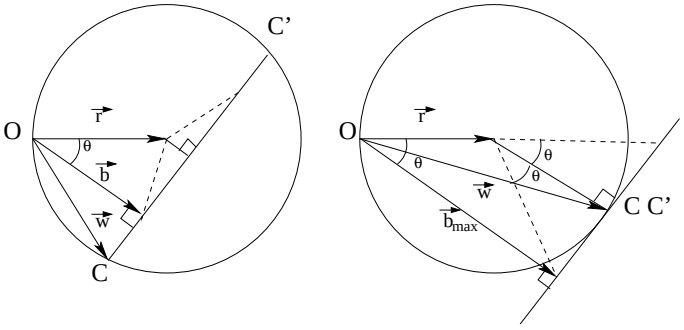

FIG. 2. Geometric construction for finding the smoothest velocity change $\vec{w}$ of the coldest atoms (with velocity $\vec{v}_C$ in the hotter region and the hottest atoms (with velocity $\vec{v}_H$ in the colder region. Both figures represent a sphere of radius $\vec{r} = (\vec{v}_C - \vec{v}_H)/2$. The plane perpendicular to $\vec{b}$, intersects the sphere in a circle, which is the locus of solutions $\vec{w}$ obeying energy and momentum conservation rules. The points C and C' (in the $\vec{r}$–$\vec{b}$ plane) give the solutions with least and greatest impulse. The right-hand version shows the largest vector $\vec{b}$ which allows solutions for $\vec{w}$. The minimum and maximum impulse solutions have merged to a point.

$\dot{e}(\ell) > 0 > \dot{e}(N_S/2-\ell) = -\dot{e}(\ell)$. Find the coldest atom (meaning least kinetic energy) of all atoms of mass m_i in the hotter slab, denoting its velocity as $\vec{v}_C$. Find the hottest atom of the same mass in the colder slab, denoting its velocity $\vec{v}_H$. Given the large fluctuations of the Maxwell-Boltzmann ensemble, it is certain that $v_H^2 > v_C^2$. Choose an appropriate velocity $\vec{w}$ and add it to the velocity $\vec{v}_C$ and subtract it from $\vec{v}_H$:

$$\begin{aligned} \vec{v}_H &\to \vec{v}_H - \vec{w} \\ \vec{v}_C &\to \vec{v}_C + \vec{w} \end{aligned} \tag{8}$$

The same operation should be done for the pair of slabs $-\ell$ and $\ell - N_S/2$. All slabs can be done simultaneously, or different random times can be used for different slabs.

There are three criteria for an appropriate $\vec{w}$, which uniquely fix the desired choice. (i) The cold atom's kinetic energy should increase by Δ, an energy that can be specified in advance as $(\dot{e}\tau)\cos(2\pi\ell/N_S)$, where τ is the average time interval between random interventions. (ii) The hot atom's kinetic energy should decrease by Δ. Then both momentum and energy are conserved. Heating has the desired form $\dot{e}\cos(2\pi\ell/N_S)$ with $\dot{e}$ chosen not too different from $k_BT/N_S\tau$. Trial calculations should test for the best choices of $\dot{e}$ and τ. (iii) There is still a one-dimensional family of vectors $\vec{w}$; from these, choose the smallest $|\vec{w}|$, which gives the least impulse to the affected atoms.

The energy shift criteria (i) and (ii) give equations $-2\vec{v}_H\cdot\vec{w} + w^2 = -2\Delta/m \equiv -\delta$, and $2\vec{v}_C\cdot\vec{w} + w^2 = +\delta$. Adding and subtracting these equations give

$$\begin{aligned} \delta &= (\vec{v}_H + \vec{v}_C)\cdot\vec{w} \\ w^2 &= (\vec{v}_H - \vec{v}_C)\cdot\vec{w}, \end{aligned} \tag{9}$$

a linear and a quadratic equation for $\vec{w}$. These have a simple geometric interpretation shown in Fig. 2. The first equation restricts the projection of $\vec{w}$ along the vector $\vec{v}_H + \vec{v}_C$. Geometrically, this means that $\vec{w}$ lies on the plane (shown by C, C' in Fig. 2) perpendicular to the vector $\vec{b} \equiv \delta(\vec{v}_C + \vec{v}_H)/|\vec{v}_C + \vec{v}_H|^2$, where the origin of $\vec{w}$ coincides with the origin of $\vec{b}$. The second equation restricts $\vec{w}$ to the surface of a sphere of radius $|\vec{v}_H - \vec{v}_C|/2$, centered at the end of the vector $\vec{r} \equiv (\vec{v}_H - \vec{v}_C)/2$, whose origin also coincides with the origin of $\vec{w}$. The sphere and the plane intersect on a circle, indicated by C, C' in Fig. 2. This circle is the one-dimensional family of solutions $\vec{w}$ satisfying Eqs.(9). It is also clear from the geometry that the shortest vector $\vec{w}$ (the one that satisfies criterion (iii)) is the one shown, from O to C. This lies in the same plane as the two known vectors $\vec{r}$ and $\vec{b}$ (also the same plane as $\vec{v}_H$ and $\vec{v}_C$). Therefore

$$\begin{aligned} \vec{w} &= \alpha\vec{r} + \beta\vec{b} \\ \vec{r} &= (\vec{v}_H - \vec{v}_C)/2 \\ \vec{b} &= \frac{\delta(\vec{v}_H + \vec{v}_C)}{|\vec{v}_H + \vec{v}_C|^2}. \end{aligned} \tag{10}$$

These definitions allow Eqs.(9) to be written as

$$\begin{aligned} b^2 &= \vec{w} \cdot \vec{b} \\ w^2 &= 2\vec{r} \cdot \vec{w}. \end{aligned} \tag{11}$$

The solution for $\vec{w}$ is

$$\begin{aligned} \beta &= 1 - \alpha\frac{\vec{r} \cdot \vec{b}}{b^2} \\ \alpha &= 1 - \sqrt{1 - X} \\ X &= \frac{(b^2 - 2\vec{b} \cdot \vec{r})b^2}{b^2 r^2 - (\vec{b} \cdot \vec{r})^2} \end{aligned} \tag{12}$$

To derive this, substitute Eq.(10) for $\vec{w}$ in terms of the unknown coefficients α and β into the Eqs.(9). The linear equation is used to find β in terms of α. Eliminating β in favor of α in the quadratic equation gives a quadratic equation for α. The appropriate solution is displayed in Eq.(12). An alternate version directly in terms of the velocities $\vec{v}_H$ and $\vec{v}_C$ is

$$X = (2\Delta/m)\frac{(2\Delta/m) - (v_H^2 - v_C^2)}{v_H^2 v_C^2 - (\vec{v}_H \cdot \vec{v}_C)^2} \tag{13}$$

$$\vec{w} = \frac{\alpha}{2}(\vec{v}_H - \vec{v}_C) + \left[\frac{2\Delta}{m} - \frac{\alpha}{2}(v_H^2 - v_C^2)\right]\frac{\vec{v}_H + \vec{v}_C}{|\vec{v}_H + \vec{v}_C|^2} \tag{14}$$

Notice that X in Eq.(13) has a non-negative denominator that becomes zero in an accidental event where $\vec{v}_H$ and $\vec{v}_C$ are parallel; X is then ill-defined, because no solution exists. An alternate pair of C and H atoms must be chosen. In the simulations reported in subsequent sections, we find that Δ should be chosen small, making the numerator of X in Eq.(13) negative. Thus both X and α are negative, contrary to the version shown in Fig. 2. This does not adversely affect anything.

There is a second solution, $\alpha = 1 + \sqrt{1 - X}$, corresponding to the maximum $|\vec{w}|$, designated as C' in Fig. 2. For $|\vec{b}| > b_{\max}$, there are no real solutions. This corresponds to $X > 1$. The condition for the two solutions to coincide is $X = 1$, which agrees with $b_{\max} = r(1 + \cos\theta)$, where θ is the angle between $\vec{b}$ and $\vec{r}$. This can be understood from the right hand part of Fig. 2, illustrating the case where the circle collapses to a point. For reasonable choices of the parameter $m\delta/2 = \Delta$, meaning values smaller than or similar to $k_B T/N_S$, solutions should always exist.

V. TEST ON LENNARD-JONES LIQUID

The LJ liquid is a simple case, used by Müller-Plathe[8] to test his algorithm. The pair potential is

$$V_{\rm LJ} = 4\epsilon\left[\left(\frac{\sigma}{r}\right)^{12} - \left(\frac{\sigma}{r}\right)^{6}\right] \tag{15}$$

The parameters for argon are ϵ/k_B = 119.6K and σ =3.405Å. First, we reproduce Müller-Plathe's results, at the same (N, V, T)= 2592 atoms, $\rho = N/V = 0.849/\sigma^3$, and $T = 0.7\epsilon/k_B$ =84K. The same simulation cell is used, of dimension 10.06 × 10.06 × 30.18 σ^3, with periodic boundary conditions. The cut-off distance for the LJ potential is 3.0σ. We get the same answer, κ=7.1 in LJ units.

As shown in Fig. 2 of ref. 8, and confirmed by our calculation in Fig. 3, the temperature gradient is essentially constant all the way to, and including, the slabs 0 and $N_S/2 = 10$. This is because thermal conductivity in a liquid is very local. This can be contrasted with fig. 6 of ref. 10 or fig. 4 of ref. 3, for crystals with non-local κ. Gas theory is certainly not correct for a liquid; the concept of a mean-free path is not valid. However, we can get an idea of what happens by unlicensed use of the gas formula $\kappa = C\bar{v}\Lambda/3$. The measured thermal conductivity of liquid argon (0.132 W/mK at temperature near 100K and pressure near 1Mbar[11,12]) then corresponds to a mean free path $\Lambda \approx 0.14$ Å, more than 30 times smaller than the slab separation $d = 1.51\sigma$. In other words, the non-local conductivity $\kappa(x - x')$ decays to zero by the first neighbor slab, or $\kappa(q)$ is independent of q out to values of q larger than $q_{\max} = \pi/d$.

Also shown in Fig. 3 is the sinusoidal temperature profile gotten numerically from our sinusoidal heating. The computational system is unaltered. The 2592 atoms are in the same cell, divided into 20 slabs, at the same T. Sinusoidal heat $N_S\dot{e}$ between 1 and 5 $\epsilon/\Delta t$ is used. The interval between heat injections is $\Delta t = 60\delta t$, where the time step of the "velocity Verlet" Newton's-law integration algorithm[13,14] is $\delta t = 0.007 t_{LJ}$. The Lennard-Jones unit of time for argon is $t_{LJ} = \sigma\sqrt{(m/\epsilon)} = 2.16$ ps. Equi-

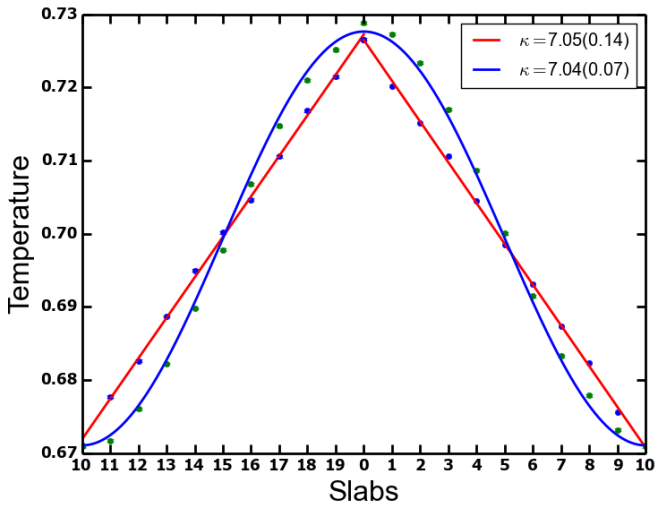

FIG. 3. temperature profiles from direct simulations for the Lennard-Jones crystal. The points fit by the straight line are a reproduction of the calculation of Müller-Plathe. The points fit by the sine curve use the same simulation cell, and spatially sinusoidal heating and cooling.

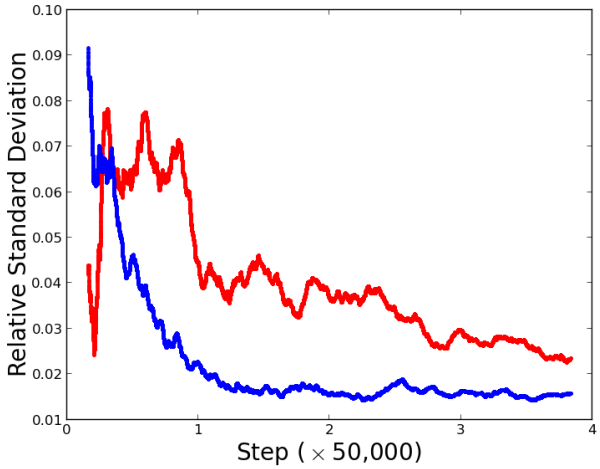

FIG. 4. Time evolution of the error of simulation of κ for the Lennard-Jones liquid. The upper and noisier curve uses the method of Müller-Plathe. The lower curve is the result of the sinusoidal algorithm of this paper.

libration required 10^4 δt of constant T simulation, and $T(\ell)$ averaging was done for $2\times10^5\delta t$; good convergence was found in $5\times10^4\delta t$ as shown in Fig. 4.

To estimate errors, consider that there are 130 atoms per slab, each with mean energy k_BT and rms deviation of k_BT from the mean, according to Maxwell-Boltzmann statistics. Thus the mean slab energy per atom, at any particular moment, should be about $k_BT \pm k_BT/\sqrt{130}$ Therefore, if averaged over 100 random and independent thermalized configurations, the temperature error in a slab will be less than 1%. A run of $5\times10^4\delta t$ should be more than sufficient for this purpose. Fig. 3 suggests errors of order $0.001k_BT$ in the slab temperatures.

Compared with the Müller-Plathe[8] result, both of the current ones give the same value, $\kappa = 7.1$ in LJ units, which is 0.133 W/mK, very close to the experimental value for argon, 0.132 W/mK[11,12]. The sinusoidal algorithm gives faster convergence and a slightly more accurate final answer, as shown in Fig 4.

VI. EXTRAPOLATION

MD answers for κ are computed for finite size L. Therefore extrapolation is required to estimate the bulk ($L\to\infty$) answer. Sellan *et al.*[15] have analyzed this. It was also analyzed in the previous paper[3], using a Debye model. Here we continue the analysis. Equations (22,23) of ref. 3 are

$$\kappa(q) = \frac{1}{\Omega}\sum_Q \hbar\omega_Q \frac{\partial n_Q}{\partial T} v_{Qx}^2 \tau_Q \cos^2(qd/2) F(q,\Lambda_{Qx}) \quad (16)$$

$$F(q,\Lambda) = \left[1 + 4\sin^2(qd/2)\left\{\left(\frac{\Lambda}{d}\right) + \left(\frac{\Lambda}{d}\right)^2\right\}\right]^{-1}, \quad (17)$$

where v_{Qx}, τ_Q, and $\Lambda = v_{Qx}\tau_Q$ are the group velocity, quasiparticle lifetime, and x-component of mean free path of the phonon mode of frequency ω_Q. These equations solve the PBE in relaxation-time approximation for the case where heat is applied as $\cos(q\ell d)$ with $q = 2\pi/L$ and where L is the periodic repeat length an infinite sample or of a model on a torus (exactly as in the calculations of secs. V and VII). In ref. 3, these were approximately evaluated using a Debye model, and integrating Q over a Debye sphere. The Debye version is

$$\kappa_D(q) = \kappa_{D0}\cos^2(qd/2)\frac{1}{N}\sum_Q \left(\frac{Q_x}{Q}\right)^2\left(\frac{Q_D}{Q}\right)^p F(q,\Lambda_{Qx}), \quad (18)$$

where κ_{D0} is a convenient scale factor,

$$\kappa_{D0} = \frac{3N}{\Omega}k_B v^2 \tau_D, \quad (19)$$

and the mean free path is

$$\Lambda_{Qx} = v\tau_D \frac{Q_x}{Q}\left(\frac{Q_D}{Q}\right)^p. \quad (20)$$

The Debye wavevector has its usual value, $(6\pi^2N/\Omega)^{1/3}$, and the exponent p is chosen to be 2.

Here, instead of integrating over the Debye sphere, we do the discrete sum of Eq. 18 over the Brillouin zone of the *fcc* simulation cell that will be used in the next section for the LJ crystal. That is, we use only those $\vec{Q}$'s in the *fcc* Brillouin zone such that $\exp(i\vec{Q}\cdot\vec{A}_i) = 1$, where $\vec{A}_i$, for

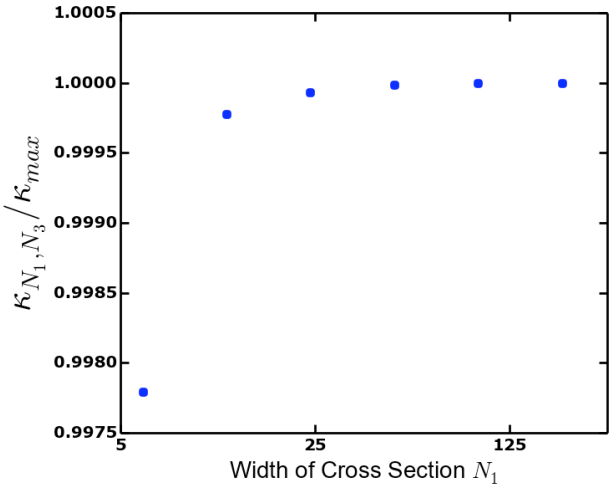

FIG. 5. Fast convergence of κ expected for a simulation cell of size N_1, N_1, N_3, as predicted using the Debye-model version of Eqs.(16,17). The Q-sum is not over the Debye sphere, but over the anisotropic Q-mesh corresponding to the normal modes of the *fcc* crystalline LJ lattice. The value $N_3 = 500$ was fixed, and $\kappa_{\max}$ is set to the value with $N_1 = 500$.

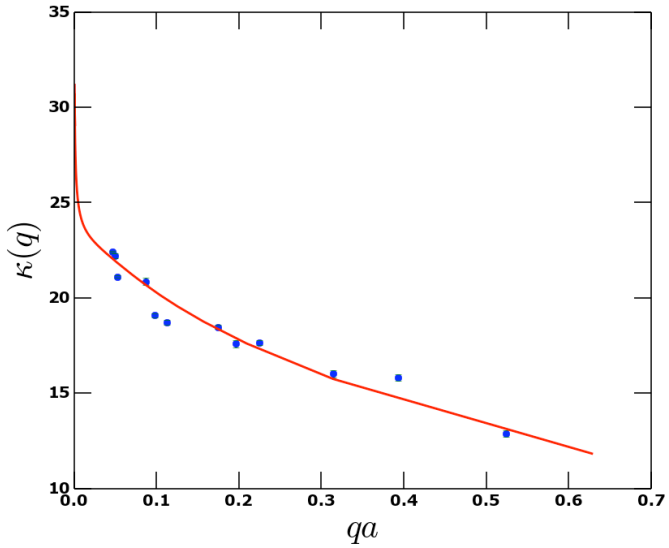

FIG. 6. Just an illustration. The Debye model is used to model expected convergence versus supercell length L. The figure will have only one curve. It doesn't need to be this tall. The Q-sum is not over the Debye sphere, but over the anisotropic Q-mesh corresponding to the normal modes of the *fcc fcc* LJ supercell. The values $N_1 = N_2 = 6$ are fixed, and $\kappa_{\max}$ is set to the value with $N_3 = 500$.

$i = 1, 2, 3$, are the orthogonal translation vectors of the simulation supercell. As an example, the mesh used in Sec. V for the LJ liquid corresponds to $\vec{A}_1 = 6a(1, 0, 0)$, $\vec{A}_2 = 6a(0, 1, 0)$, and $\vec{A}_3 = 18a(0, 0, 1)$, where $a = 1.68\sigma$ is the lattice constant of the *fcc* conventional cubic cell, using the liquid argon density, $0.849/\sigma^3$. Our simulation cells in this and the next section will be very similar, but longer in the $\vec{A}_3$ direction, and with a readjusted to 1.56σ to give the higher density[14,16], $1.053/\sigma^3$, of the low pressure LJ crystal. The corresponding $\vec{Q}$'s are the vectors $\ell\vec{G}_1 + m\vec{G}_2 + n\vec{G}_3$ of the lattice reciprocal to the $\vec{A}$'s. This is an anisotropic reciprocal-space mesh, being coarse in the directions $\vec{A}_1$ and $\vec{A}_2$, but finer in the direction $\vec{A}_3$, corresponding to the actual distribution of normal modes of the atoms in the simulation cell of the LJ crystal. Our hypothesis is that the Debye model, with frequency $\omega_Q = v|\vec{Q}|$ for all 3 branches, and $1/\tau_Q = (1/\tau_D)(Q/Q_D)^2$, will sufficiently capture the physics of the LJ crystal for purposes of learning how to extrapolate to infinite simulation cell size. Then we will use this result to guide extrapolation of the simulations in the next section.

First we study convergence as a function of the transverse dimension of the cell. The result, shown in Fig. 5, is extremely favorable, indicating that coarseness of the $\vec{Q}$-mesh in the $\vec{A}_1$ and $\vec{A}_2$ directions is no problem.

Next we study convergence as a function of the longitudinal dimension of the cell. Here convergence is slower. **Figure needed.** Fig. 6 is inserted here just for temporary illustration. The result is very similar (?) to what was found in ref.3 where Debye-model spherical symmetry was exploited and the mesh was isotropic.

VII. LENNARD-JONES CRYSTAL

For an LJ crystal, the situation is different. Phonon gas theory applies to fairly good approximation. Higher energy phonons have mean free paths longer than the slab thickness d, which we choose to be $a = 5.32\mathring{A}$. Lower energy phonons have mean free paths Λ_Q increasing, roughly as $1/\omega_Q^2$. The values of Λ_Q are not as long as in GaN, modeled by Zhou *et al.*[10]. Doing a converged calculation by MD methods is challenging. **Need to read and cite prior calculations.** We use this to test whether our algorithm is helpful. The time step of the "velocity Verlet" Newton's-law integration algorithm[13,14] is $\delta t = 0.007t_{LJ}$ for shorter samples, and $0.014t_{LJ}$ for longer samples.

At T not too far above the triple-point temperature, higher than second-order anharmonicity starts to be noticable in LJ crystals. This shortens the mean free paths, to the point where gas theory starts to break down. This has two advantages: the simulation cell does not have to be as long, and non-Boltzmann behavior is the regime where an MD simulation is worth doing . We have chosen to simulate crystalline LJ argon at T=80K, close to the experimental triple point (84K and 0.7 atmospheres.)

Fig.7 shows results for $\kappa(q = 2\pi/L)$ where $L = N_3 d$ is the length of the simulation cell, and $d = a$. These calculations used a heat input $\dot{e}\tau$ of 1.265ϵ, the interval τ being $60\delta t$. **(Yerong – am I guessing correctly what you mean?)**

The value of κ in argon at T =80 K is measured[17] to

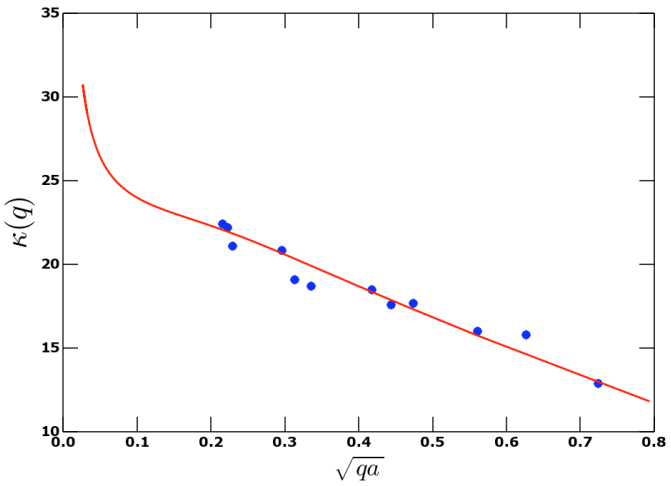

FIG. 7. Fourier-space $\kappa(q)$ computed numerically at the minimum $q_{\min} = 2\pi/L$ for various cell sizes L. The values of κ are shown in LJ units ($\kappa_{\rm LJ} = (k_B/\sigma^2)\sqrt{(\epsilon/M)}$= 0.0188 W/mK). **Yerong – could you explain how exactly you chose the red curve? Thanks.**

be in the range 0.4 to 0.6 W/mK. The value of 22 in LJ units obtained from Fig.7 corresponds to 0.41 W/mK.

Appendix A: Homogeneous Mesh

Equations 16 and 17, when combined, are

$$\kappa(q) = \frac{1}{\Omega}\sum_Q \hbar\omega_Q \frac{\partial n_Q}{\partial T} v_{Qx}^2 \tau_Q \frac{\cos^2(qd/2)}{1+4\sin^2(qd/2)(\Lambda/d)^2} \tag{A1}$$

The term first order in Λ/d is dropped because the corrections in the denominator are only important when $\Lambda/d = v\cos\theta\tau_D(Q_D/Q)^p/d$ is large, and the quadratic term dominates. In classical approximation, $\hbar\omega_Q\frac{\partial n_Q}{\partial T} \to k_B$, and in Debye approximation, $v_{Qx} = v\cos\theta$. We are interested in the minimum wavevector $q = 2\pi/L$, so $\cos(qd/2) \to 1$ and $2\sin(qd/2)\Lambda/d \to 2\pi\Lambda/L$. Then Eq. A1 becomes (for the special case $p = 2$)

$$\kappa(q_{\min}) = \frac{k_B v^2\tau_D}{\Omega}\sum_Q \frac{\cos^2\theta(Q_D/Q)^2}{1+\cos^2\theta\lambda^2(Q_D/Q)^4} \tag{A2}$$

where $\lambda \equiv 2\pi v\tau_D/L = 2\pi\ell_{\min}/L$. In Debye approximation, for a uniform and dense mesh (*i.e.* a large crystal), the sum becomes

$$\sum_Q \to \frac{3\Omega}{(2\pi)^3}2\pi\int_0^{Q_D} dQQ^2\int_{-1}^{1} d\cos\theta, \tag{A3}$$

where the factor 3 is for the three modes. After performing the angular integral, A2 becomes

$$\begin{aligned}\kappa(q_{\min}) &= \frac{3k_B v^2\tau_D}{2\pi^2\lambda^2}\int_0^{Q_D} dQ\frac{Q^4}{Q_D^2} \\ &\times\left[1-\frac{1}{\lambda}\left(\frac{Q}{Q_D^2}\right)^2\tan^{-1}\lambda\left(\frac{Q_D}{Q}\right)^2\right] \\ &= \frac{3\kappa_{D,0}}{2\lambda^2}\int_0^1 duu^{3/2}\left[1-\frac{u}{\lambda}\cot^{-1}\frac{u}{\lambda}\right].\end{aligned} \tag{A4}$$

Here the replacements have been made $u = (Q/Q_D)^2$ and $\tan^{-1}(1/x) = \cot^{-1}x$, and the conductivity scale $\kappa_{D,0} = 3Nk_Bv^2\tau_D/\Omega$ is used.

Next we assert the following identity, best proved by direct differentiation:

$$\begin{aligned}h(u) &= \frac{7}{2}\int du\left[u^{3/2}-\frac{u^{5/2}}{\lambda}\cot^{-1}\frac{u}{\lambda}\right] \\ &= u^{5/2}+2\lambda^2u^{1/2}-\frac{u^{7/2}}{\lambda}\cot^{-1}\frac{u}{\lambda} \\ &-\frac{\lambda^{5/2}}{\sqrt{2}}\left[\frac{1}{2}\log\left(\frac{u+\sqrt{2u\lambda}+\lambda}{u-\sqrt{2u\lambda}+\lambda}\right)+\tan^{-1}\left(\frac{\sqrt{2u\lambda}}{\lambda-u}\right)\right]\end{aligned} \tag{A5}$$

Now we have an answer,

$$\kappa(q_{\min}) = \frac{3}{7}\frac{\kappa_{D,0}}{\lambda^2}[h(1)-h(0)] \tag{A6}$$

It is necessary to be careful in evaluating $h(1)-h(0)$. As we integrate u from 0 towards 1 (as in Eq.A4), all the terms in the integral, Eq.A5 have smooth behavior except the last term, $\tan^{-1}[\sqrt{(2u\lambda)}/(\lambda-u)]$. Note that $0 < \lambda < 1$ since L is large. Therefore, in this term, the argument of the arctangent increases from zero to $+\infty$, where the arctangent equals $\pi/2$, then switches to $-\infty$, with the arctangent still equal to $\pi/2$, and finally increases toward 0 from the negative side, with the arctangent approaching π from the negative side. Therefore, the value of $\tan^{-1}[\sqrt{(2u\lambda)}/(\lambda-u)]$ at $u = 1$ is $\pi-\tan^{-1}[\sqrt{(2\lambda)}/(1-\lambda)]$. The answer is thus

$$\begin{aligned}\frac{7\lambda^2}{3\kappa_{D,0}}\kappa(q_{\min}) &= 1+2\lambda^2-\frac{\tan^{-1}\lambda}{\lambda} \\ &-\frac{\lambda^{5/2}}{\sqrt{2}}\left[\frac{1}{2}\log\left(\frac{1+\sqrt{2\lambda}+\lambda}{1-\sqrt{2\lambda}+\lambda}\right)+\pi-\tan^{-1}\left(\frac{\sqrt{2\lambda}}{1-\lambda}\right)\right]\end{aligned} \tag{A7}$$

Finally, at large sample size L, the smallest mean free path $\ell_{\min} = v\tau_D$ is small compared with L. The parameter λ is $2\pi\ell_{\min}/L$ and the leading size-dependent correction is

$$\kappa(q_{\min}) = \frac{5}{7}\kappa_{D,0}\left(1-\frac{3\pi}{5}\sqrt{\frac{\pi\ell_{\min}}{L}}\right). \tag{A8}$$

This result confirms the conjecture of Ref. 3 that numerical result might be best extrapolated by plotting κ *versus* $\sqrt{(1/L)}$.

Appendix B: Inhomogeneous mesh

Now our task is to reconsider how Eq. A1 behaves in a finite size crystal or simulation cell, when one dimension ($L_z \equiv L$) gets large but the other two ($L_x = L_y \equiv L_{xy}$) remain small. The answer is, a new non-analytic piece occurs, and rather than converging to the $L \to \infty$ limit as $1/\sqrt{L}$ (found above for the homogeneous mesh), it diverges as $\sqrt{L}$. These results are specific to the power law relaxation $\tau_Q = \tau_D(\omega_D/\omega)^p$ with $p = 2$. The divergence is a property of a one-dimensional wire, indicating that ballistic transport has a dominant effect in such a system. As the width L_xL_y of the wire increases, the divergent term in $\kappa(q_{\rm min})$ decreases as a^2/L_xL_y, restoring the better-behaved homogeneous answer.

The specific system under consideration is an fcc crystal of volume $Na^3/4$, where a is the conventional primitive cube size, $N = 4N_xN_yN_z$ is the total number of atoms, N_x and N_y being small integers held fixed, and N_z being a large integer. We seek the behavior as N_z gets very large. The conductivity is given by Eq. A2, rewritten as

$$\frac{\kappa(q_{\rm min})}{\kappa_{D,0}} = \frac{1}{N}\sum_{Q_z}\sum_{Q_x,Q_y}\frac{(Q_z/Q)^2(Q_D/Q)^2}{1+(Q_z/Q)^2\lambda^2(Q_D/Q)^4}, \quad \text{(B1)}$$

where $\lambda = 2\pi\ell_{\rm min}/L$, $\ell_{\rm min}$ being the mean free path of the highest frequency phonons. The Q-vectors are $\vec{Q} = (2\pi/a)(n_x/N_x, n_y/N_y, n_z/N_z)$. This choice is required to make vibrational normal modes satisfy periodicity in the supercell. There are N Q-vectors in the Brillouin zone. The Debye model simplifies summation over the Brillouin zone by using the Debye sphere, with a volume equal to n time the volume of the primitive Brillouin zone, n being the number of atoms in the primitive cell, 4 for fcc. The Q-points are dense along the z direction and sparse in the others. Only the Q_z-sum can be turned into an integral. It is consistent with the philosophy of the Debye model, to not use a sphere in this case, but a cube-shaped Brillouin zone, of volume n times $(2\pi/a)^3$. The Q_z sum is then an integral, going from the smallest non-zero Q_z, $2\pi/L$, ending at the largest, $Q_D = n^{1/3}\pi/a$, and multiplied by 2 to cover both negative and positive Q_z.

$$\frac{\kappa(q_{\rm min})}{\kappa_{D,0}} = \frac{1}{N_xN_y}\sum_{Q_x,Q_y}\frac{a}{\pi}\int_{2\pi/L}^{Q_D} dQ\frac{(Q_z/Q)^2(Q_D/Q)^2}{1+(Q_z/Q)^2\lambda^2(Q_D/Q)^4} \quad \text{(B2)}$$

The number of terms in the Q_x, Q_y sum is $\approx n^{2/3}N_xN_y$, typically 50 for an MD simulation, or a few thousand for a small nanowire. Of these terms, the one which requires special attention is the $Q_x = Q_y = 0$ term. We denote this term by $\kappa_{00}(q_{\rm min})$,

$$\begin{aligned}\frac{\kappa_{00}(q_{\rm min})}{\kappa_{D,0}} &= \frac{1}{N_xN_y}\frac{a}{\pi}\int_{2\pi/L}^{Q_D} dQ\frac{Q^2Q_D^2}{Q^4+\lambda^2Q_D^4} \\ &= \frac{n^{1/3}}{2N_xN_y}\int_{\epsilon}^{1} dx\frac{x^2}{x^4+\lambda^2}, \end{aligned} \quad \text{(B3)}$$

where the variable x is Q/Q_D and $\epsilon = 2a/n^{1/3}L$. The integral diverges as $\lambda \to 0$. Using very similar algebra to that of Appendix A, the answer is

$$\frac{\kappa_{00}(q_{\rm min})}{\kappa_{D,0}} = \frac{n^{1/3}}{2N_xN_y}\left[\frac{\pi}{2}\sqrt{\frac{L}{4\pi\ell_{\rm min}}} - 1 + \text{ terms of order } \frac{1}{L}\right] \quad \text{(B4)}$$

The Debye model is reliable as a guide for the low frequency behavior, provided the relaxation-time approximation and the associated power law p are correct. The conclusion is a bit surprising. It indicates that if anisotropic simulation cells are used for "direct" MD simulation of κ, then the extrapolation to very long cells suffers from an unintended 1D singularity. The product N_xN_y should increase approximately as rapidly as $N_z^{1/2}$ to prevent this term distorting the extrapolated answer. In actual simulations, this is probably more a sobering thought than a serious warning. But the effect is real, and shows up in the Debye-model numerics shown in Figs. 6 and 7

III. ACKNOWLEDGEMENTS

We thank A. J. H. McGaughey for helpful advice. We thank the Stony Brook University Institute for Advanced Computational Science (IACS) for time on their computer cluster. This work was supported in part by DOE grant No. DE-FG02-08ER46550.

* philip.allen@stonybrook.edu
† li.yerong@smail.nju.edu.cn

[1] D. N. Payton, M. Rich, and W. M. Visscher, Phys. Rev. **160**, 706 (1967).
[2] P. K. Schelling, S. R. Phillpot, and P. Keblinsky, Phys. Rev. B **65**, 144306 (2002).
[3] P. B. Allen, Phys. Rev. B **90**, 054301 (2014).
[4] G. D. Mahan and F. Claro, Phys. Rev. B **38**, 1963 (1988).
[5] Z. Liang and P. Keblinski, Phys. Rev. B **90**, 075411 (2014).
[6] D. G. Cahill *et al.*, Appl. Phys. Rev. **1**, 011305 (2014).
[7] P. B. Allen and J. L. Feldman, Phys. Rev. B **48**, 12581 (1993).

[8] F. Müller-Plathe, J. Chem. Phys. **106**, 6082 (1997).
[9] B.-Y. Cao and Y.-W. Li, J. Chem. Phys. **133**, 024106 (2010).
[10] X. W. Zhou, S. Aubry, R. E. Jones, A. Greenstein, and P. K. Schelling, Phys. Rev. B **79**, 115201 (2009).
[11] B. A. Younglove and H. J. M. Hanley . Phys. Chem. Ref. Data **15**, 1323 (1986); G. A. Cook, *Argon, Helium and the Rare Gases*, Intersciences: NY, 1961.
[12] H. J. M. Hanley, R. D. McCarthy, and W. M. Hayes, J. Phys. Chem. Ref. Data **3**, 979 (1974); H. Ziebland and T. Burton, Brit. J. Appl. Phys. **9**, 52 (1958).
[13] J. P. Hansen and L. Verlet, Phys. Rev. **184**, 151 (1969).
[14] M. E. Tuckerman, B. J. Berne, and G. J. Martyna, J. Chem. Phys. **94**, 6811 (1991).
[15] D. P. Sellan, E. S. Landry, J. E. Turney, A. J. H. McGaughey, and C. H. Amon, Phys. Rev. B **81**, 214305 (2010).
[16] A. J. C. Ladd and L. V. Woodcock, Mol. Phys. **36**, 611 (1978).
[17] F. Clayton and D. N. Batchelder, J. Phys. C **6**, 1213 (1973).